Acta Pharmaceutica Sinica B 2021;11(4):1047−1055

Chinese Pharmaceutical Association
Institute of Materia Medica, Chinese Academy of Medical Sciences

Acta Pharmaceutica Sinica B

www.elsevier.com/locate/apsb
www.sciencedirect.com

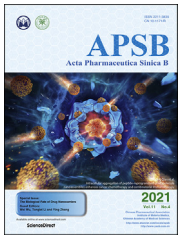

ORIGINAL ARTICLE

Uptake and trafficking of different sized PLGA nanoparticles by dendritic cells in imiquimod-induced psoriasis-like mice model

Zibei Lin[a], Long Xi[a], Shaokui Chen[a], Jinsong Tao[a], Yan Wang[b], Xin Chen[a], Ping Li[b], Zhenping Wang[c], Ying Zheng[a,*]

[a]*State Key Laboratory of Quality Research in Chinese Medicine, Institute of Chinese Medical Sciences, University of Macau, Macao 999078, China*
[b]*Beijing Hospital of Traditional Chinese Medicine, Affiliated with Capital Medical University, Beijing 100050, China*
[c]*Department of Dermatology, School of Medicine, University of California, La Jolla, San Diego, CA 92093, USA*

Received 11 June 2020; received in revised form 31 July 2020; accepted 6 August 2020

KEY WORDS

Psoriasis;
PLGA nanoparticles;
Fluorescence;
Dendritic cells;
Fluorescence resonance energy transfer;
Lymphoid organs;
Uptake and trafficking;
Biofate

Abstract Psoriasis is an autoimmune inflammatory disease, where dendritic cells (DCs) play an important role in its pathogenesis. In our previous work, we have demonstrated that topical delivery of curcumin-loaded poly (lactic-*co*-glycolic acid) (PLGA) nanoparticles (NPs) could treat Imiquimod (IMQ)-induced psoriasis-like mice. The objective of this study is to further elucidate biofate of PLGA NPs after intradermal delivery including DCs uptake, and their further trafficking in psoriasis-like mice model by using fluorescence probes. Two-sized DiO/DiI-loaded PLGA NPs of 50 ± 4.9 nm (S-NPs) and 226 ± 7.8 nm (L-NPs) were fabricated, respectively. *In vitro* cellular uptake results showed that NPs could be internalized into DCs with intact form, and DCs preferred to uptake larger NPs. Consistently, *in vivo* study showed that L-NPs were more captured by DCs and NPs were firstly transported to skin-draining lymph nodes (SDLN), then to spleens after 8 h injection, whereas more S-NPs were transported into SDLN and spleens. Moreover, FRET imaging showed more structurally intact L-NPs distributed in skins and lymph nodes. In conclusion, particle size can affect the uptake and trafficking of NPs by DCs in skin and lymphoid system, which needs to be considered in NPs tailing to treat inflammatory skin disease like psoriasis.

Abbreviations: APCs, antigen-presenting cells; CLSM, confocal laser scanning microscope; DCs, dendritic cells; DiI, 1,1′-dioctadecyl-3,3,3′,3′-tetramethylindocarbocyanine perchlorate; DiO, 3,3′-dioctadecyloxacarbocyanine perchlorate; DMF, dimethylformamide; MLN, mesenteric lymph nodes; NPs, nanoparticles; PDI, polydispersity index; PFA, paraformaldehyde; SDLN, skin-draining lymph nodes.

*Corresponding author. Fax: +853 28841358.
E-mail address: yzheng@umac.mo (Ying Zheng).

Peer review under responsibility of Chinese Pharmaceutical Association and Institute of Materia Medica, Chinese Academy of Medical Sciences.

https://doi.org/10.1016/j.apsb.2020.11.008

2211-3835 © 2021 Chinese Pharmaceutical Association and Institute of Materia Medica, Chinese Academy of Medical Sciences. Production and hosting by Elsevier B.V. This is an open access article under the CC BY-NC-ND license (http://creativecommons.org/licenses/by-nc-nd/4.0/).

© 2021 Chinese Pharmaceutical Association and Institute of Materia Medica, Chinese Academy of Medical Sciences. Production and hosting by Elsevier B.V. This is an open access article under the CC BY-NC-ND license (http://creativecommons.org/licenses/by-nc-nd/4.0/).

1. Introduction

Psoriasis refers to an immune-regulated disease resulted from immune regulatory disorder and excessive proliferation of skin cells. Incidence rate of psoriasis is reported at a range from 0.09% to 11.43% according to the WHO global report on psoriasis (WHO, 2016), where most patients are reported to be in mild to moderate situation[1]. Though the real and clear etiopathogenesis of psoriasis is still under study, it is reckoned that initial stimulation of dermal dendritic cells (DCs), with which discovery Ralph M. Steinman won the 2011 Nobel Prize in Physiology or Medicine, leads to a vast changes of keratinocytes, epidermal morphology and relevant immunological reactions[2]. Maturated DCs in the skin with a heterogeneous population can migrate and present antigens to induce activation of different T cells, leading to release of inflammatory cytokines and eventually initiate psoriasis[3–6]. Hyperproliferation of keratinocytes leads to increased thickness of skin epidermis, changes on numbers of DCs and lymphocyte infiltration, all of which lead to skin lesions[7]. Therefore, we presume that a new DCs-targeted drug delivery platform is promising to cure psoriasis through topical/transdermal administration. In our previous work, we have fabricated two particle-sized curcumin PLGA nanoparticles (NPs) and demonstrated their enhanced anti-psoriasis activity in IMQ-induced psoriasis-like mice model[8]. However, little is known about their biofate such as the DCs uptake and trafficking of these biodegradable NPs after topical/transdermal administration, especially the distribution and release/integrity of NPs.

To study the release/integrity of the NPs, currently there are several available labeling and imaging strategies, including aggregation-caused quenching (ACQ) fluorophores, aggregation-induced emission (AIE) fluorophores, and fluorescence resonance energy transfer (FRET) fluorophores. The principle of ACQ effects is that the fluorescence emitted from specific materials will be quenched owing to the aggregation of these materials at a certain concentration, which has successfully served as imaging tools to track the biofate of nanomedicine[9]. The fluorescence will change from none/weak to strong once the NPs are released. Whereas AIE shows reverse phenomenon that strong fluorescence will gradually fade as NPs are released, because AIE fluorophores will emit strong fluorescent signals when aggregation occurs. AIE performs well in imaging of *in vitro* and *in vivo* nano-based pharmaceuticals[10]. FRET refers to a pair of fluorescence probes named donor and receptor. The fluorescence will emit from receptor after receiving energy transferred from donor when the distance of these two probes are closer than 10 nm. FRET ratio is widely used to evaluate the release/integrity of drug-loaded NPs that the higher the value is, the better the integrity of the NPs[11,12].

Comparing with other administration routes, topical drugs to treat mild to moderate psoriasis include corticosteroids, retinoids, calcineurin inhibitors, vitamin D analogues, and some bioactive small molecules extracted from Chinese herbs[13]. Due to the strong skin barriers including many tight layers of the dead cells in outer stratum corneum (SC), as well as several layers of epidermis and dermis cells, except for small molecules (<500 Da) and lipophilic drugs ($0 < \mathrm{Log}P < 3$), only few drugs could be transported across the skin layer and reach to the blood, like cyclosporine, tacrolimus, etc[14,15]. Even in the psoriasis-like skin, the enhanced *in vitro* penetration of the small drug molecules and NPs below 100 nm are still very limited[16]. Therefore, intradermal injection (i.d.) of NPs into the dorsal skins of IMQ-induced psoriasis-like mice was utilized to facilitate fluorescence observation in the skin in this work. And through i.d. injection, biofate of PLGA NPs after traversing SC layers was investigated, which may provide design ideas for the development of novel topical pharmaceuticals which could overcome SC barriers in psoriasis treatment. Moreover, FRET technique has been applied to investigate both *in vitro* and *in vivo* integrity of the PLGA NPs[17].

In this study, fluorescence-labeled PLGA NPs of two particle sizes were performed as model nanocarriers to study the size effect on DCs uptake and NPs trafficking to lymphoid organs both *in vitro* and *in vivo*, as well as release/integrity of those biodegradable NPs after i.d. to IMQ-induced psoriasis-like mice dorsal skins.

2. Materials and methods

2.1. Reagents

3,3′-dioctadecyloxacarbocyanine perchlorate (DiO), 1,1′-dioctadecyl-3,3,3′,3′-tetramethylindocarbocyanine perchlorate (DiI), and Hoechst 33342 were purchased from Invitrogen (Carlsbad, CA, USA). PLGA (LA:GA = 50:50, *w/w*, 5000 Da) was obtained from Wing Hing Chemical Co., Ltd. (Hongkong, China). Tween 80 was bought from Shanghai Aladdin Bio-Chem Technology Co., Ltd. (Shanghai, China). Imiquimod was purchased as Aldara™, a topical cream (5% IMQ; Health Care Ltd., Loughborough, UK). Milli-Q water was from a Millipore Direct-Q ultra-pure water system (Millipore, Bedford, USA). Carbopol 974N was purchased from Shanghai Chineway Pharmaceutical Technology Co., Ltd. (Shanghai, China). Paraformaldehyde of 4% was purchased from Phygene Life Sciences Co., Ltd. (Fuzhou, China). Hair remover spray foam was from Dimples, Linco Care Ltd. (Carrington, MA, USA). Leica Tissue Freezing Medium was purchased from Shanghai Leibusi Biotechnology Co., Ltd. (Shanghai, China). BSA powder was bought from Beyotime Biotechnology (Shanghai, China). Fetal Bovine serum (FBS) was purchased from Thermo Fisher Scientific (Waltham, MA, USA). Antibodies PerCP-Cy5.5 anti-mouse CD45 (35-0451-82) were purchased from eBioscience™ (San Diego, CA, USA). APC anti-mouse CD11c (MCD11c05) was purchased from Invitrogen (Carlsbad, CA, USA). Anti-CD11c primary antibody (ab33483) and Goat Anti-Mouse IgG H&L (ab150115) were bought from Abcam (Cambridge, UK). All other chemical agents were of analytical grade or above.

2.2. Cell culture

JAWSII dendritic cell line (ATCC® CRL-11904™), a bone morrow-derived immature dendritic cell line, was chosen as *in vitro* cell model. JAWSII dendritic cell line was propagated in a 25 cm^2 culture flask in Alpha minimum essential medium with ribonucleosides (Gibco, α-MEM, nucleosides, 12571−063) with 10% (*v*/*v*) FBS, 10 ng/mL murine GM-CSF (Nanjing GenScript Inc., Nanjing, China) and 2% (*v*/*v*) L-glutamine (4 mmol/L) at 37 °C in a humidified atmosphere containing 5% CO_2. The growth medium was renewed once per week.

2.3. Animals

Female wild-type (WT) C57BL/6J mice (7−9 weeks old) were provided by Faculty of Health Sciences in University of Macau, China. Mice were housed in specific pathogen free (SPF) condition. All relevant experimental protocols were approved by The Animal Ethics Committee of University of Macau, China and all experiments showed below were operated according to the NIH Guidelines for the Care and Use of Laboratory Animals, USA.

2.4. Methods

2.4.1. Preparation and characterization of DiO/DiI-loaded PLGA nanoparticles

DiO/DiI-loaded PLGA NPs were prepared by anti-solvent and flash nanoprecipitation method based on our previous publication[8]. DiO/DiI and PLGA (5 mg/mL) were dissolved in DMF as organic phase, and stabilizer tween 80 (0.1%, 1 mg/mL) dissolved in diluted water was regarded as aqueous phase. Organic phase was fast injected by syringe into aqueous phase (1:9, *v*/*v*) with constant stirring on magnetic stirrer. Sizes of DiO/DiI-loaded PLGA NPs were changed by controlling the stirring speed. After finishing the preparation, the organic solvent was removed by using ultrafiltration device with a centrifugation speed at 4000 rpm (Heraeus™ Multifuge™ X3R, Thermo Fisher Scientific, Waltham, MA, USA) for 10 min. Triplicated centrifugations were made to ensure the organic solvent was totally removed. Then the prepared NPs were diluted in Milli-Q water, and the particle size, polydispersity index (PDI) and zeta potential were measured using a Malvern Zetasizer Nano-ZS system (Malvern Instruments, Worcestershire, WR, UK). Triplicated measurements were conducted for each sample. Two prepared NPs were diluted by water and dropped onto surface of a specific copper mesh and dried overnight. Finally, prepared samples were photographed using a transmission electron microscope (TEM, JEM-2100F, Tokyo, Japan).

2.4.2. Preparation of nanoparticles-loaded hydrogel

In order to be applied onto skin, the above PLGA NPs were loaded into hydrogel to improve the viscosity. Carbopol 974 N of 2% (*w*/*v*) was chosen as the blank gel, which was slowly added into the quantified solvent of DiO/DiI-loaded NPs with a constant gentle stirring on magnetic stirrer in darkness overnight. After completely swelling, the hydrogel was neutralized to pH 6−7 by dropping moderate triethanolamine. To quantify the loading amount of DiO and DiI in the hydrogel, the prepared NPs were dissolved in methanol with dilution to 100 times and transferred to micro-plate reader (FlexStation III Multi-Mode Microplate Reader, San Jose, CA, USA). The excitation wavelength was 484 and 549 nm for DiO and DiI, respectively, while the emission wavelength was 501 nm for DiO and 565 nm for DiI, respectively.

2.4.3. Cellular uptake of DiI-loaded PLGA nanoparticles

JAWSII dendritic cells (CRL-11904) were seeded in a 12-well plate at a density of 1.0×10^5 per well. DiI-loaded PLGA NPs (S-NPs or L-NPs) were added into α-MEM at a final DiI concentration of 5 μg/mL, and incubated with cells for 1, 2 and 4 h, respectively. The medium was abandoned and cells were digested next washed in PBS for 3 times, and then mean fluorescence intensity was detected by BD Accuri C6 flow cytometer with the C6 Software (BD Biosciences, San Jose, CA, USA). Triplicated independent experiments were conducted to ensure reproducibility. Data were analyzed and presented as mean ± standard deviation (SD).

2.4.4. In vitro evaluation of integrity by using FRET

JAWSII dendritic cells were seeded in a 12-well plate, where cell-climbing films (cells grew on a glass slice purchased from Shanghai Leibusi Biotechnology Co., Ltd., Shanghai, China) were laid in wells in advance. Each well was seeded with a cell density of 1×10^5 cells/mL. Two kinds of DiO/DiI-loaded PLGA NPs (S-NPs and L-NPs) prepared above were added into culture medium at a concentration of 10 μg/mL (DiO/DiI) and incubated for 1 h. Cells were then washed three times by PBS, and fresh α-MEM was added into the wells. Four time points at 0, 1, 2 and 4 h were set to observe the cellular uptake of S-NPs and L-NPs. The cell-climbing films were carefully removed out using a pair of forceps and fixed in 4% paraformaldehyde (PFA) for 10 min, then rinsed in PBS for 3 times, subsequently stained with Hochest 33342 (10 μg/mL) for 10 min and washed for another 3 times before being covered with the slices and made into glass slides so as to be observed by confocal laser microscope (CLSM, Leica TCS SP8 multi-photon microscope, IL, USA). FRET technique performs well in studying the intracellular and *in vivo* behaviors of nanomedicines[18] as in Eq. (1):

$$\text{FRET ratio} = \frac{I_{\text{receptor}}}{I_{\text{receptor}} + I_{\text{donor}}} \tag{1}$$

where I_{receptor} refers to fluorescence intensity at maximum absorption wavelength of receptor probe, I_{donor} refers to that of donor probe. The gain for every channel was invariant during the whole scanning course. Images of FRET channel were obtained by utilizing an excitation wavelength of 488 nm and the emission wavelengths between 580 and 650 nm. For lambda scan, the spectral analysis conditions were set that the emission wavelength range was between 500 and 650 nm with an excitation wavelength of 488 nm in each ROI, where 10 nm intervals with an acquisition mode of xyλ were recorded. The images were captured by CLSM and fluorescence intensity quantification was analyzed by Leica Application Suite X software (Buffalo Grove, IL, USA). The calculation of FRET ratio was presented as mean ± SD ($n = 3$).

2.4.5. Establishment of IMQ-induced psoriasis-like mice

Aldara™ was first served as a stimulus to induce mice localized skin and systemic inflammation by activating toll-like receptor 7 in 2009[19]. The mouse model of psoriasis form dermatitis was well established by repeated topical administration Aldara™ (5% IMQ) and successfully built in our previous research[16,20]. Around 25% (*w*/*w*) cream in the Aldara™ product equals to ~62.5 mg was consecutively applied to mice dorsal skins every day for 7 days. The active compound was equivalent to a dose of ~3 mg/mouse/day.

2.4.6. *In vivo integrity monitoring in skins and skin-draining lymph nodes (SDLN)*

The IMQ-induced psoriasis-like mice were divided into two groups, where equivalent NPs (2.55 μg DiO in 75 μL, multi-point injection) of S-NPs and L-NPs were intradermally injected into psoriasis-like mice dorsal skins. The cages were wrapped with dark plastic bags to avoid lights, and then mice were sacrificed at 1, 2, 4, and 8 h post administration. Mice dorsal skins and SDLN were collected and a small piece of skin (0.5 cm × 0.5 cm) and whole lymph nodes of each mouse was processed into sections with a thickness of 10 μm. Intact sections were first put into 4% PFA for 10 min, then stained with Hochest 33342 (10 μg/mL) for 10 min. Each rinse/wash lasted for 5 min and triplicated during whole course. Finally, they were made into prepared microscope slices and observed by CLSM. A line-by-line basis was applied to scan the slices. Autofluorescence was cut by controlling the channel gain. Then gain for every channel was invariant during the whole imaging course. Images of FRET channel were acquired under same conditions described in Section 2.4.4.

2.4.7. *Trafficking of DiO-loaded PLGA nanoparticles in vivo*

2.4.7.1. Immunofluorescence staining and imaging. The IMQ-induced psoriasis-like mice were divided into two groups with same manipulations as described in Section 2.4.6. Subsequently, mice were sacrificed at 1, 4, 8, 24 and 48 h post administration. Mice dorsal skins were freshly excised into small pieces and washed in PBS with three times, each time lasted for 5 min. Immunostaining was performed to find out the colocalization of DCs with NPs. Vertical sections were cut at the thickness of 10 μm. Then skin sections were fixed with 4% paraformaldehyde for 15 min, following by 5% BSA incubation for 1 h at ambient temperature, and then incubated overnight at 4 °C with anti-CD11c primary antibody (ab33483, Abcam, 1:200). After 1 h incubation with goat anti-mouse IgG H&L (ab150115, Abcam, 1:500) at room temperature, nuclear staining was performed using Hochest 33342 (10 μg/mL). Skin sections were eventually observed by using CLSM at an excitation wavelength of 488 nm and emission wavelengths between 500 and 530 nm for DiO channel detection. Immunofluorescence was observed at an excited wavelength with an Alexa Fluor® 647 filter.

2.4.7.2. Flow cytometric analysis. The IMQ-induced psoriasis-like mice were divided into three groups, two of which were conducted with same manipulations as described in Section 2.4.6. The other group was treated with equivalent PBS as control group. Subsequently, mice were sacrificed at 1, 4, 8, 24 and 48 h post administration. Mice lymphoid organs, including SDLN, mesenteric lymph nodes (MLN) and spleens, were freshly excised and immersed in PBS with 1% FBS. Then those tissues were grinded and filtered with 70 μm cell screens to obtain single-cell suspension. Samples were stained with anti-CD45 antibody (35-0451-82, eBioscience™), anti-CD11c (MCD11c05, Invitrogen™) for 30 min at 4 °C. Samples were run on BD LSRFortessa™ (Becton, Dickinson and Company, Franklin Lakes, NJ, USA) and different cell subsets were analyzed by FlowJo software (Tree Star Inc., Ashland, OR, USA).

2.4.7.3. In vivo imaging system (IVIS). The group division and treatment of mice were depicted in Section 2.4.6. Biodistribution of PLGA NPs was observed in freshly collected tissues and organs (blood, heart, liver, spleen, SDLN and kidney) after treated for 1, 2, and 4 h with an IVIS 200 system (Caliper Life Sciences, MA, USA).

2.4.8. *Statistical analysis*

All data were presented as mean ± SD except for specific indication. One-way ANOVA was performed to analyze comparisons of data of more than two groups with GraphPad Prism 7.0. (GraphPad, San Diego, CA, USA).

3. Results and discussion

3.1. *Characterization of DiO/DiI-loaded PLGA nanoparticles*

Fluorescence-labeled PLGA NPs of two sizes were prepared. Their characterizations were displayed in Fig. 1. The mean particle size of the smaller (S-NPs) and larger NPs (L-NPs) were at 50 ± 4.9 and 226 ± 7.8 nm, respectively. All of the PLGA NPs showed a spherical shape without apparent aggregation when observed from TEM images in Fig. 1. Besides, small PDI values indicated the good homogeneity of S-NPs and L-NPs, which are 0.21 ± 0.05 and 0.16 ± 0.03, respectively. The zeta potential of S-NPs is −19.1 ± 2.0 mV, and that of L-NPs is −20.0 ± 1.0 mV, showing a good nanoparticle stability.

3.2. *Dendritic cells uptake and integrity evaluation of two-sized PLGA nanoparticles*

To observe the different uptake behaviors of two-sized NPs in DCs, DiI-loaded PLGA NPs (DiI: 5 μg/mL) of S-NPs and L-NPs were individually incubated with DCs for 1, 2 and 4 h. As shown in Fig. 2A and B, the fluorescence of cells for both S-NPs and L-NPs were increased over the incubation time, suggesting the accumulation of NPs in DCs with time. However, higher fluorescence intensity could be detected in DCs incubated with L-NPs compared to that with smaller one. It demonstrated that DCs preferred to uptake larger nanoparticles. Our findings are consistent to other researchers' reports where DCs were reported to show a size-dependent uptake of gold NPs and amphiphilic poly NPs *in vitro*[21,22].

To determine the integrity of different-sized NPs after being internalized into the DCs, DiO/DiI-loaded NPs (S-NPs and L-NPs) were respectively pre-incubated with DCs for 1 h as the starting point, and then the medium was removed and fluorescence was observed at different time intervals up to 4 h. As shown in Fig. 2C, the red fluorescence of FRET channel demonstrated the intact uptake of the two sized NPs into DCs. By using confocal microscopy lambda scan as a full spectrum analysis to calculate FRET ratio (Fig. 2D), we observed that all the FRET ratio values were decreased over time. The FRET ratio values of S-NPs and L-NPs declined to ∼0.4 and ∼0.5 after 4 h exposure, respectively, suggesting that all the NPs were gradually disassembled in DCs where S-NPs showed faster disassembled rate with time.

3.3. *Few topically administered nanoparticles could penetrate into psoriasis-like mice skin*

As shown in Supporting Information Fig. S1A, epidermis and dermis of mice skin were distinguished by white dotted lines. After topical administration of two-sized DiO/DiI-loaded PLGA NPs hydrogels on psoriasis-like mice skin, weak fluorescence signal in DiO and FRET channel could be observed only in SC

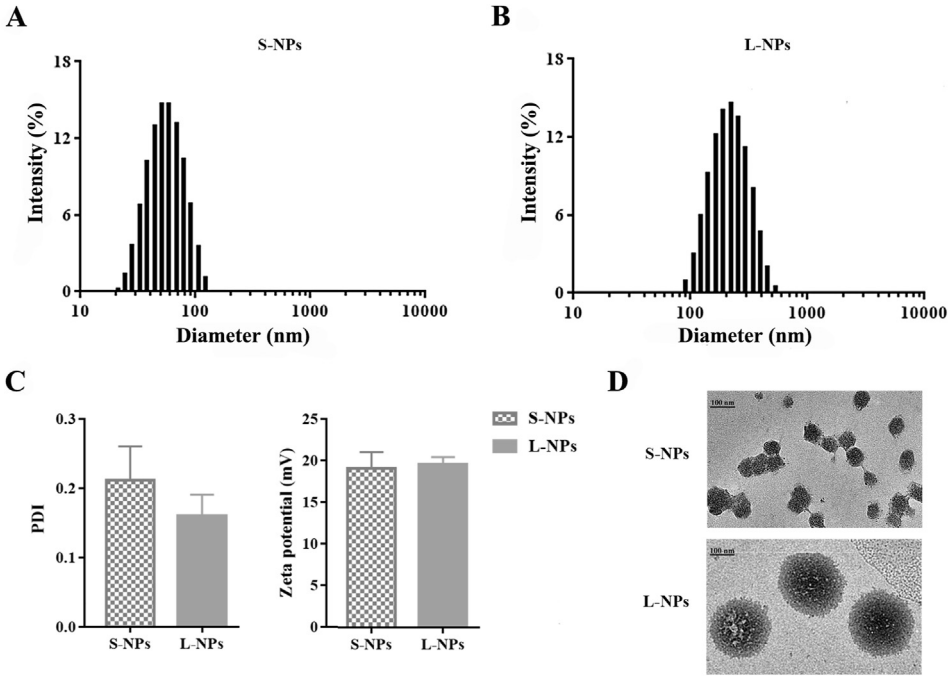

Figure 1 Characterization of DiO/DiI-loaded PLGA nanoparticles. Size distribution of S-NPs (A) and L-NPs (B), and their zeta potential and PDI. Data are presented as mean ± SD ($n = 3$) (C). (D) TEM images of S-NPs and L-NPs. Scale bar = 100 nm.

and upper epidermis layers of the skin, where the fluorescence intensity of the S-NPs were apparently higher than those of the L-NPs. In L-NPs-treated group, more fluorescence signal can be observed in skin SC and hair follicles as the arrows indicated, suggesting that L-NPs were mostly accumulated in epidermis and hair follicles but could not reach to the dermis layer. Red FRET channel still can be observed after 4 h post administration, which demonstrated that some integral NPs still existed but slowly dissociated with time. All of above results indicated that although S-NPs showed a little better penetration ability when compared to L-NPs *in vivo*, and few PLGA NPs could penetrate across the psoriasis-like skin barrier by topical administration of the hydrogels to mice. In another NPs penetration research of our group, *ex vivo* dorsal skins were applied and smaller NPs showed better

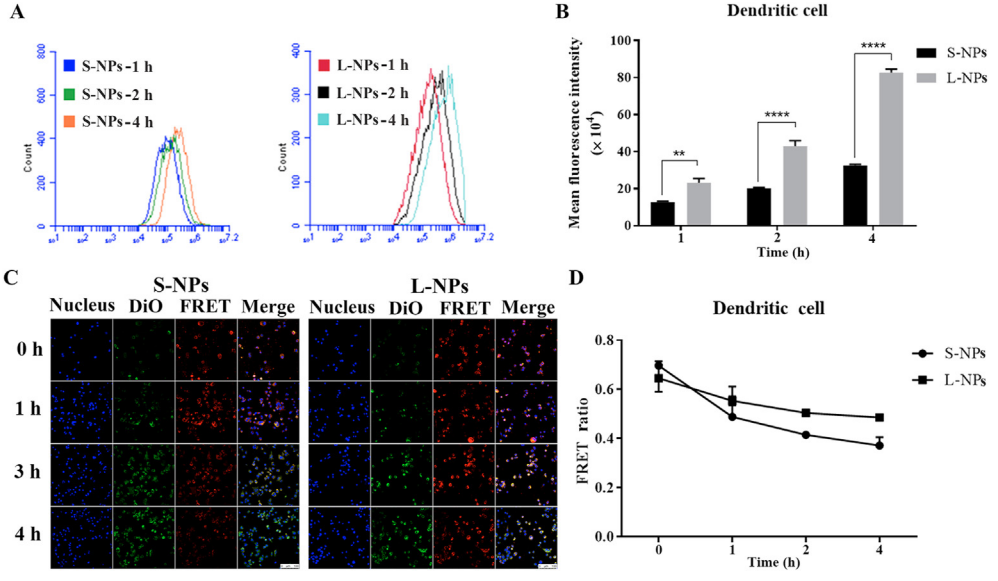

Figure 2 Comparison of cellular uptake and integrity of two different-sized PLGA nanoparticles. (A) Counts of DCs that absorbed DiI-loaded PLGA nanoparticles (DiI: 5 μg/mL) after co-incubated with S-NPs (left) and L-NPs (right) for 1, 2 and 4 h. (B) Mean fluorescence intensity of DCs incubated with DiI-loaded PLGA nanoparticles (DiI: 5 μg/mL) for 1, 2 and 4 h, respectively. Data are presented as mean ± SD ($n = 3$), $^{****}P < 0.0001$, $^{**}P < 0.01$. (C) Confocal laser scanning imaging of DCs, which were respectively pre-incubated with DiO/DiI-loaded PLGA nanoparticles (DiO/DiI: 10 μg/mL) for 1 h as the starting point, and then medium was removed to observe the FRET up to 4 h. (Scale bar = 100 μm). (D) FRET ratio changes with time for S-NPs and L-NPs. Data are presented as mean ± SD ($n = 3$).

penetration effectiveness as well[16]. However, even in psoriasis-like skin, the SC and epidermis were still effective obstacles to prevent majority of particles from penetrating into the skin. It is well known that the SC layer is composed of dead keratinocytes and combined with the tight junction to form a hydrophilic barrier only allowing molecules less than 500 kDa with suitable hydrophilicity (log$P$ 1−2) to penetrate across the skin[23].

Previous publications have demonstrated nano-vehicles or drug molecules that are successfully dispersed to skin dermis could be captured by antigen-presenting cells (APCs) and presented to T cells, leading to activated immune response[24,25]. To further elucidate whether NPs can be transported to immune-related organs in psoriasis-like mice model, DiO-loaded PLGA nanoparticles of smaller sizes were loaded into hydrogel and topically applied to psoriasis-like mice. Then mice were sacrificed to collect SDLN, MLN and spleens for flow-cytometry analysis. As shown in Fig. S1B, the particle-positive cells from these organs are around 1% and showed no significant changes with time when compared to the control group (without drug administration), indicating that not enough particles can be accurately quantified in these lymphoid organs. These results further suggested that few PLGA NPs could penetrate into skin and then delivered to lymphatic organs by topical delivery of PLGA hydrogel.

3.4. *Dendritic cells uptake and trafficking of different sized nanoparticles after intradermal injection*

To improve the amount of the NPs in the skin for fluorescence observation and accurate quantification, two sized NPs were intradermally injected into dorsal skins of IMQ-induced psoriasis-like mice, respectively, which will overcome the SC layer and allow larger amount of PLGA nanoparticles getting into skin epidermis. This investigation can provide *in vivo* data as reference and inspirations when designing transdermal drugs administered by overcoming SC layer (like, intradermal injection, microneedle or other non-invasive strategies). To study interactions between the NPs and DCs, both skin and SDLN sections were stained with specific antibody CD11c in red to track the membrane protein of DCs. As shown in Fig. 3A and B, DiO-loaded PLGA NPs with green fluorescence were accumulated in the skin dermis (Fig. 3A), and then transported to SDLN (Fig. 3B). The green fluorescence probe DiO-loaded PLGA NPs were partially co-localized with DCs stained with red fluorescence, suggesting that some of the NPs were captured by DCs after i.d. administration. Quantification of particle uptake by DC populations in different lymphoid organs was then performed by flow cytometry. Based on the results of DC-particle double positive cells in SDLN shown in Fig. 3D, DCs preferred to uptake L-NPs but not S-NPs with time. In addition, as displayed in Fig. 3E, apparently higher DCs-particle positive populations could be quantified in spleens of L-NPs-treated groups. DCs play a crucial role in etiopathogenesis of psoriasis for its antigen-presenting nature. Previous study has demonstrated that once skin got irritated by external insults, a significant increase of DCs will be observed in dermis and the amount of DCs migrated to SDLN got promoted as well[21]. In the inflamed skin, when NPs were injected by i.d. to dermis layer, DCs can perform their antigen-presenting nature to capture external antigen and induce the expansion of clonal, and then prime T cell response[5]. Similarly, researchers have put forward a novel idea of intradermally injected DC-targeted vaccines to cure T cells-related fatal diseases, like HIV, malaria and tuberculosis[26].

In general, skin epidermis lacks of capillary vessels, serving as a barrier to prevent particulates entering dermis. However, the dermis is comprised of collagen, extracellular matrix proteins, subcutaneous fat and secondary structures like hair follicles, nerve fibers, sudoriferous glands, blood capillaries and lymphatic vessels[27]. These secondary structures can trap nanocarriers and drugs topically administered and prolong their retention time as a reservoir[28]. Therefore, fluorescence of NPs (green) remained pretty strong even after 48 h administration as shown in Supporting Information Fig. S2.

The blood vessels and lymphatics in the dermis support the immune cells-like DCs, macrophages and T cells to infiltrate in dermis, which offer the topically administered nanocarriers and drugs an access to systemic circulations. However, under the condition of inflammation like psoriasis, the skin structure greatly changes. The angiogenesis occurs and lymphatic vessels are dramatically increased in psoriasis lesion area[29], which may provide more chances for NPs to enter into lymphatic or blood circulation. As shown in Supporting Information Fig. S3A, strong green fluorescence can be observed after i.d. administration for both S-NPs and L-NPs-treated groups, while the green fluorescence intensity of both two groups faded over time, suggesting the elimination process of the NPs in SDLN. Furthermore, quantification of particle transportation to different lymphoid organs was analyzed by flow cytometry. As shown in Fig. S3B, compared to L-NPs-treated group, higher proportion of particle-positive cells were detected in SDLN from S-NPs-treated mice under the same condition, indicating that more amount of S-NPs were transported to SDLN than L-NPs. Moreover, the S-NPs transported into SDLN gradually reached to a peak after 8 h treatment and then dropped down with time, whereas the L-NPs reached to the peak at 24 h post treatment, suggesting that S-NP were faster absorbed to SDLN than L-NPs. Similarly, as shown in Figs. S3C and a dramatic increase of S-NPs was detected in spleens after administration for 8 h, while L-NPs reached to the peak with more time at 24 h, suggesting that both sized NPs were subsequently delivered to the spleen. Because higher proportion of particle-positive cells was detected both in SDLN and spleens from mice treated with S-NPs, indicating that smaller NPs were easier to be delivered to lymphoid organs. The possible explanation may be that diameter of lymphatic vessels allows particles between 10 and 100 nm to pass through[30]. Therefore, except *via* DCs uptake of NPs and migration to the lymphoid organs, the smaller size may also facilitate S-NPs to diffuse into lymphoid capillaries. Whereas for L-NPs, intact NPs have no access to lymphoid capillaries but free probes may enter to lymphoid flow after release. Additionally, as shown in Supporting Information Fig. S3D, particles-positive cells in MLN of L-NPs-treated mice showed no difference when compared to IMQ-only group, whereas that in S-NPs-treated group displayed statistical significance at 24 and 48 h post administration. However, the particle-positive cells of MLN are all below 2%, indicating that little amount of S-NPs were transported to MLN.

Furthermore, *in vivo* images of mice organs were conducted using the same treatment as above and displayed in Supporting Information Fig. S4. Weak fluorescence were apparent in liver, while much stronger signal has been observed in SDLN after mice being treated with S-NPs for 1 h. Livers, SDLN and spleens play important roles in lymphatic circulation and lymphatic fluids flow reciprocally[6,31,32]. However, weak signal can only be observed in blood of S-NPs-treated mice after 1 h administration, and no signals can be observed in other groups with time. These results

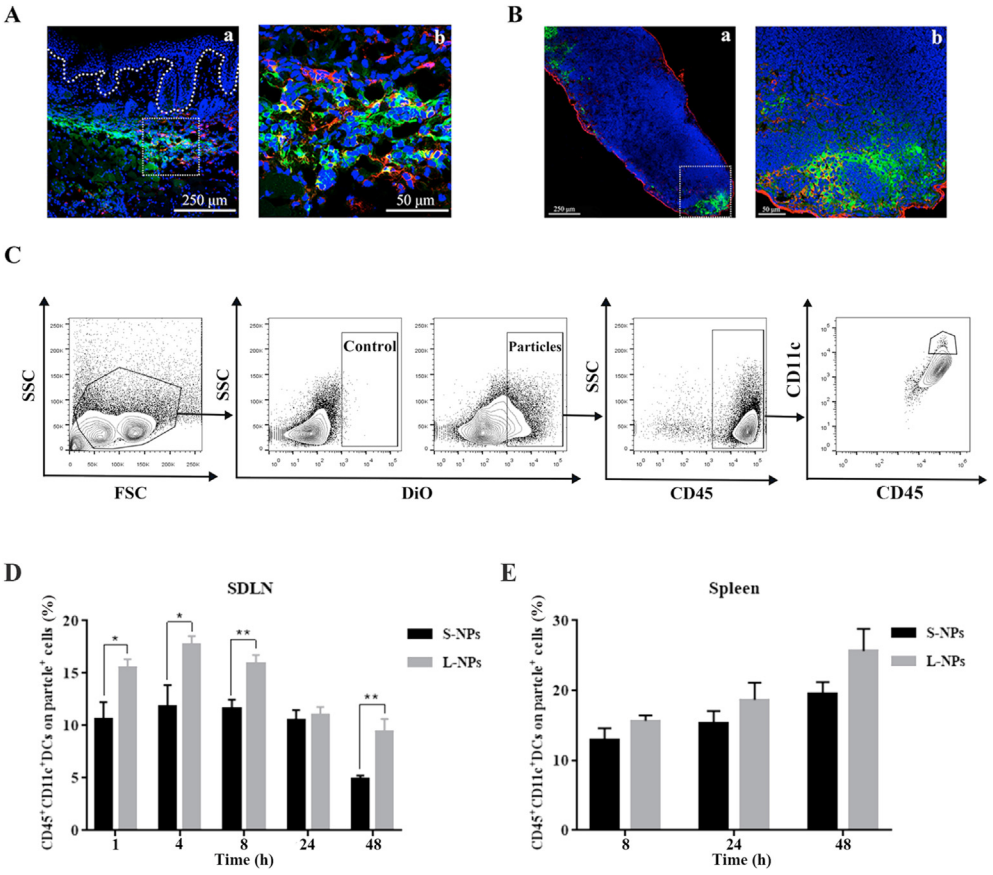

Figure 3 DCs uptake preference of intradermal injected DiO-loaded PLGA nanoparticles in IMQ-induced psoriasis-like mice. (A) Representative immunofluorescence staining of psoriasis-like mice skin section (a) that intradermally injected with DiO-loaded PLGA nanoparticles (after injection for 4 h), enlarged in (b). (B) Representative immunofluorescence staining of SDLN from psoriasis-like mice that intradermally injected with DiO-loaded PLGA nanoparticles (after injection for 1 h), enlarged in (b). Scale bar: 250 μm (enlargement: 50 μm). Blue: nucleus, green: DiO, red: anti-CD11c. (C) Flow cytometry gating strategy to identify and analyze DCs populations in different lymphoid organs. Gating is shown in one representative data of mice at 1 h exposure after treated with S-NPs. After the initial live gating in a forward scatter (FSC) and side scatter (SSC) plot, particle-positive cells were first gated. Among them, DCs from SDLN and spleens were gated in a CD45 *versus* CD11c plot. (D) PBS controls and different sizes of DiO-loaded PLGA nanoparticles were intradermally administrated in IMQ-induced psoriasis-like mice, and the single-cell suspensions obtained from lymphoid organs were analyzed at 1, 4, 8, 24, and 48 h after particle exposure. Among particle-positive subset in SDLN (D) and spleens (E), comparison between S-NPs and L-NPs detected in these tissues were made. Data are presented as mean ± SEM ($n = 6$), $^{**}P < 0.01$, $^{*}P < 0.05$.

may indicate that transportation of NPs to livers and SDLN were dominantly *via* lymphatic drainage but not through the blood circulation. Therefore, we can presume that L-NPs (~200 nm) hardly enter into blood circulation, which can cause less systemic adverse effects and more focus on lymphatic immune system. Besides, compared to the group of S-NPs, there existed a time lag to observe the fluorescence signals in the SDLN and spleens in group treated with L-NPs, which may due to their different transport pathways. It is reasonable to hypothesize that the main pathway for S-NPs traveling to SDLN and spleens is *via* entering lymphatic capillaries in skin dermis but not the DC migration as S-NPs reached the organs more quickly. Besides, another possible explanation is that S-NPs had a relatively faster released speed than L-NPs where more free probes diffused into lymphoid capillaries and transported by lymphatic flow. As previous studies revealed that larger NPs preferred to be captured by APCs and then migrated to draining lymph nodes[33,34], DCs uptake and migration may be the main pathway for L-NPs entering into the organs. However, more experiments need to be conducted to further track the delivery pathway of the S-NPs *in vivo*. In short, for the design of those anti-psoriatic agents that work by regulating the downstream immune reaction *via* targeting DCs, both the *in vitro* and *in vivo* results suggest that NPs with larger size will be preferred under the circumstance that SC is overcome. Whereas for anti-psoriatic nanomedicine with topical administration, suitable methods should be considered to overcome SC barrier and improve nanoparticle skin penetration.

3.5. *In vivo integrity of DiO/DiI-loaded PLGA nanoparticles*

Study on the biofate of NPs is fundamental to find out how the drug takes effects. However, *in vivo* behaviors of NPs are complicated due to the complex microenvironments changes[35]. For nanomedicine, especially those designed to target specific organs, efficient delivery is essential. To observe the NPs integrity over time, SDLNs from IMQ-induced psoriasis-like mice that were intradermal injected with two-sized DiO/DiI-loaded PLGA NPs were harvested and made into sections. As shown in Fig. 4A

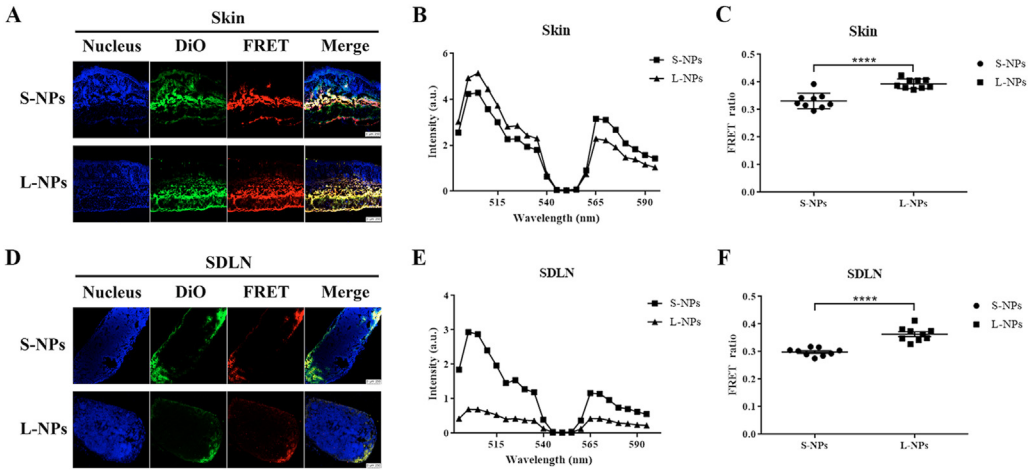

Figure 4 *In vivo* integrity of DiO/DiI-loaded PLGA nanoparticles in skins and SDLN after IMQ-induced psoriasis-like mice were intradermally injected of different-sized DiO/DiI-loaded PLGA nanoparticles at 8 h. Confocal laser scanning imaging of IMQ-induced psoriasis-like mice dorsal skins (A), and SDLN (D). Scale bar = 250 nm. Lambda scan was shown as spectrum in one representative experiment of skin sections (B), and SDLN sections (E). FRET ratios were calculated by the emission intensities of donor (505 nm) and acceptor (565 nm) based on formula FRET ratio = $I_{565\ nm}/(I_{505\ nm} + I_{565\ nm})$ and shown data pooled from separate experiments of skin sections (C), and SDLN sections (F). Data are presented as mean ± SD ($n = 9$), ****$P < 0.0001$.

and D, after treated for 8 h, fluorescence in both the DiO and FRET channel could be clearly observed in confocal laser images of skins and SDLN, indicating there are still intact nanoparticles after 8 h injection where energy transfer happened in FRET DiO and DiI pairs. Then the Lambda scan of FRET pair in skins and SDLN after treated with S- and L-NPs for 8 h were presented in Fig. 4B and E, respectively. Based on these spectral scans, FRET ratios were calculated and displayed in Fig. 4C and F. After 8 h treatment, FRET ratios of S-NPs were approximately 0.33 in skin and decreased to 0.29 in SDLN, while those of L-NPs were around 0.4 in skin and decreased to 0.36 in SDLN. Compared to S-NPs, L-NPs showed higher FRET ratio values in both skins and SDLN, which indicated that S-NPs got faster dissociated. These FRET results suggested that partial PLGA NPs could maintain intact in lymphoid organs such as SDLN after 8 h i.d. administration, which may provide a potential sustained drug release delivery system to treat immune- or lymphatic-related diseases. Thus, for design of targeted agents treating psoriasis, L-NPs will have a more retentive ability as integral particles.

4. Conclusions

In this study, we have provided the solid evidence of size-dependent uptake and trafficking patterns of PLGA NPs by DCs into SDLN and spleens. DCs uptake and transportation of S-NPs and L-NPs performed a different behavior. L-NPs were kept longer in skin dermis and more favored to be internalized by DCs both *in vitro* and *in vivo*. Thus, particulate size is a key parameter determining the uptake and trafficking by skin DC populations, which may affect downstream immune responses[36]. To increase DCs targeted rate and reduce systemic side-effects, NPs with larger particle size is preferred. Additionally, FRET results in skins and SDLN suggested that L-NPs had a slower *in vivo* dissociated speed, indicating a better sustained release ability. These findings may have important implications on tailor-made nanoparticles by controlling their particle size and improve their uptake by DCs to treat psoriasis and other immuno-related skin diseases by approaches that could overcome SC layer for sufficient nanoparticle accumulation in the skin.

Acknowledgments

This work was supported by research grants from the Macau Science and Technology Development Fund (0013/2018/A1, China) and University of Macau (MYRG2017-00200-ICMS & MYRG2019-00032-ICMS, China). We thank to the members of FHS Animal Facility at the University of Macau for experimental and technical supports. We appreciate the help of Meng Xu on drawing graphic abstract.

Author contributions

Ying Zheng contributed to the design, discussion and writing of the manuscript. Zibei Lin finished all experiments, analyzed data and drafted the manuscript. Long Xi and Shaokui Chen participated in animal experiments and data analysis. Jinsong Tao provided FRET-related experimental techniques. Yan Wang helped to provide flowcytometry analysis support. Zhenping Wang, Ping Li and Xin Chen as consultors provided suggestions on experiment design and discussion.

Conflicts of interest

The authors confirm that this article content has no conflicts of interest.

Appendix A. Supporting information

Supporting data to this article can be found online at https://doi.org/10.1016/j.apsb.2020.11.008.

References

1. Danielsen K, Olsen A, Wilsgaard T, Urberg AS. Is the prevalence of psoriasis increasing? A 30-year follow-up of a population-based cohort. *Br J Dermatol* 2013;**168**:1303−10.
2. Nestle FO, Di Meglio P, Qin JZ, Nickoloff B. Skin immune sentinels in health and disease. *Nat Rev Immunol* 2009;**9**:679−91.
3. Zaba LC, Fuentes-Duculan J, Eungdamrong NJ, Abello MV, Novitskaya I, Pierson KC, et al. Psoriasis is characterized by accumulation of immunostimulatory and Th1/Th17 cell-polarizing myeloid dendritic cells. *J Invest Dermatol* 2009;**129**:79−88.
4. Singh TP, Zhang HH, Borek I, Wolf P, Hedrick MN, Singh SP, et al. Monocyte-derived inflammatory Langerhans cells and dermal dendritic cells mediate psoriasis-like inflammation. *Nat Commun* 2016;**7**:13581.
5. Clausen BE, Stoitzner P. Functional specialization of skin dendritic cell subsets in regulating T cell responses. *Front Immunol* 2015;**6**:534.
6. Worbs T, Hammerschmidt SI, Forster R. Dendritic cell migration in health and disease. *Nat Rev Immunol* 2017;**17**:30−48.
7. Terhorst D, Chelbi R, Wohn C, Malosse C, Tamoutounour S, Jorquera A, et al. Dynamics and transcriptomics of skin dendritic cells and macrophages in an imiquimod-induced, biphasic mouse model of psoriasis. *J Immunol* 2015;**195**:4953−61.
8. Sun L, Liu ZY, Wang L, Cun DM, Tong HH, Yan R, et al. Enhanced topical penetration, system exposure and anti-psoriasis activity of two particle-sized, curcumin-loaded PLGA nanoparticles in hydrogel. *J Control Release* 2017;**254**:44−54.
9. Qi JP, Hu XW, Dong XC, Lu Y, Lu HP, Zhao WL, et al. Towards more accurate bioimaging of drug nanocarriers: turning aggregation-caused quenching into a useful tool. *Adv Drug Deliv Rev* 2019;**143**:206−25.
10. Wang YF, Zhang YX, Wang JJ, Liang XJ. Aggregation-induced emission (AIE) fluorophores as imaging tools to trace the biological fate of nano-based drug delivery systems. *Adv Drug Deliv Rev* 2019;**143**:161−76.
11. Dai TC, Jiang K, Lu WY. Liposomes and lipid disks traverse the BBB and BBTB as intact forms as revealed by two-step Forster resonance energy transfer imaging. *Acta Pharm Sin B* 2018;**8**:261−71.
12. Li Y, Song XN, Yi X, Wang RB, Lee SMY, Wang XQ, et al. Zebrafish: a visual model to evaluate the biofate of transferrin receptor-targeted 7 peptide-decorated coumarin 6 micelles. *Acs Appl Mater Inter* 2017;**9**:39048−58.
13. Meng SK, Lin ZB, Wang Y, Wang ZP, Li P, Zheng Y. Psoriasis therapy by Chinese medicine and modern agents. *Chin Med* 2018;**13**:16.
14. Eisen D, Ellis CN, Duell EA, Griffiths CEM, Voorhees JJ. Effect of topical cyclosporine rinse on oral lichen planus. *J N Engl J Med* 1990;**323**:290−4.
15. Woo DK, James WD. Topical tacrolimus: a review of its uses in dermatology. *Dermatitis* 2005;**16**:6−21.
16. Sun L, Liu ZY, Lin ZB, Cun DM, Tong HH, Yan R, et al. Comparison of normal *versus* imiquimod-induced psoriatic skin in mice for penetration of drugs and nanoparticles. *Int J Nanomed* 2018;**13**:5625.
17. Chen TK, He B, Tao JS, He Y, Deng HL, Wang XQ, et al. Application of Förster Resonance Energy Transfer (FRET) technique to elucidate intracellular and *in vivo* biofate of nanomedicines. *Adv Drug Deliv Rev* 2019;**143**:177−205.
18. Chen TK, Li CW, Li Y, Yi X, Wang RB, Lee SMY, et al. Small-sized mPEG PLGA nanoparticles of schisantherin A with sustained release for enhanced brain uptake and anti-Parkinsonian activity. *ACS Appl Mater Interfaces* 2017;**9**:9516−27.
19. van der Fits L, Mourits S, Voerman JS, Kant M, Boon L, Laman JD, et al. Imiquimod-induced psoriasis-like skin inflammation in mice is mediated *via* the IL-23/IL-17 axis. *J Immunol* 2009;**182**:5836−45.
20. Meng SK, Sun L, Wang L, Lin Z, Liu ZY, Xi L, et al. Loading of water-insoluble celastrol into niosome hydrogels for improved topical permeation and anti-psoriasis activity. *Colloids Surf B* 2019;**182**:110352.
21. Tomic S, Ethokic J, Vasilijic S, Ogrinc N, Rudolf R, Pelicon P, et al. Size-dependent effects of gold nanoparticles uptake on maturation and antitumor functions of human dendritic cells *in vitro*. *PLoS One* 2014;**9**:e96584.
22. Kim H, Uto T, Akagi T, Baba M, Akashi M. Amphiphilic poly (amino acid) nanoparticles induce size-dependent dendritic cell maturation. *Adv Funct Mater* 2010;**20**:3925−31.
23. Brown MB, Traynor MJ, Martin GP, Akomeah FK. Transdermal drug delivery systems: skin perturbation devices. In: Jain KK, editor. *Drug delivery systems*. Totowa: Humana Press; 2008. p. 119−39.
24. Su R, Fan WF, Yu Q, Dong XC, Qi JP, Zhu QG, et al. Size-dependent penetration of nanoemulsions into epidermis and hair follicles: implications for transdermal delivery and immunization. *Oncotarget* 2017;**8**:38214−26.
25. Vogt A, Combadiere B, Hadam S, Stieler KM, Lademann J, Schaefer H, et al. 40 nm, but not 750 or 1,500 nm, nanoparticles enter epidermal $CD1a^{+}$ cells after transcutaneous application on human skin. *J Invest Dermatol* 2006;**126**:1316−22.
26. Kastenmüller W, Kastenmüller K, Kurts C, Seder RA. Dendritic cell-targeted vaccines —hope or hype?. *Nat Rev Immunol* 2014;**14**:705−11.
27. Wong R, Geyer S, Weninger W, Guimberteau JC, Wong JK. The dynamic anatomy and patterning of skin. *Exp Dermatol* 2016;**25**:92−8.
28. Lademann J, Richter H, Schanzer S, Meinke MC, Darvin ME, Schleusener J, et al. Follicular penetration of nanocarriers is an important penetration pathway for topically applied drugs. *Der Hautarzt* 2019;**70**:185−92.
29. Cliff S, Bedlow AJ, Stanton AW, Mortimer PS. An *in vivo* study of the microlymphatics in psoriasis using fluorescence microlymphography. *Br J Dermatol* 1999;**141**:392.
30. Trevaskis NL, Kaminskas LM, Porter CJH. From sewer to saviour—targeting the lymphatic system to promote drug exposure and activity. *Nat Rev Drug Discov* 2015;**14**:781−803.
31. Cueni LN, Detmar M. The lymphatic system in health and disease. *Lymphatic Res Biol* 2008;**6**:109−22.
32. Ohtani O, Ohtani Y. Lymph circulation in the liver. *Anat Rec* 2008;**291**:643−52.
33. Shima F, Uto T, Akagi T, Baba M, Akashi M. Size effect of amphiphilic poly(γ-glutamic acid) nanoparticles on cellular uptake and maturation of dendritic cells *in vivo*. *Acta Biomater* 2013;**9**:8894−901.
34. Manolova V, Flace A, Bauer M, Schwarz K, Saudan P, Bachmann MF. Nanoparticles target distinct dendritic cell populations according to their size. *Eur J Immunol* 2008;**38**:1404−13.
35. Lane LA, Qian X, Smith AMS, Nie S. Physical chemistry of nanomedicine: understanding the complex behaviors of nanoparticles *in vivo*. *Annu Rev Phys Chem* 2015;**66**:521−47.
36. Zhang YN, Lazarovits J, Poon W, Ouyang B, Nguyen LNM, Kingston BR, et al. Nanoparticle size influences antigen retention and presentation in lymph node follicles for humoral immunity. *Nano Lett* 2019;**19**:7226−35.